Elementary Catastrophe's Chaos in One-Dimensional Discrete Systems Based on Nonlinear Connections and Deviation Curvature Statistics

Yamasaki, Kazuhito

(Citation)
International Journal of Bifurcation and Chaos,34(08):2430017

(Issue Date)
2024-06-15

(Resource Type)
journal article

(Version)
Accepted Manuscript

International Journal of Bifurcation and Chaos

Elementary Catastrophe's Chaos in One-Dimensional Discrete Systems Based on Non-Linear Connections and Deviation Curvature Statistics

Kazuhito Yamasaki
Department of Planetology, Graduate School of Science, Kobe University, Nada, Kobe 657-8501, Japan
yk2000@kobe-u.ac.jp

Received (to be inserted by publisher)

This study shows, by means of numerical analysis, that the characteristics of discrete dynamical systems in which chaos and catastrophe coexist are closely related to the geometric statistics in Finsler geometry. The two geometric statistics introduced are non-linear connections information, denoted as N_I, and the mean deviation curvature, denoted as $\overline{P}$. The quantity N_I can be used to determine the occurrence of chaos in terms of non-equilibrium stability. The resulting chaos is characterized by $\overline{P}$ in terms of the trajectory's robustness, which is related to the localization or globalization of chaos. The characteristics of catastrophe-induced chaos are clearly visualized through the contour topography of N_I, in which an abrupt change is represented by cliff topography (i.e., a line of critical points); initial dependence is reflected in the reversibility of topographic patterns. On overlaying the contour topography with the singularity pattern, it is evident that chaos does not arise around the singular point. Furthermore, the extensive development of cusp and butterfly chaos demands information on the non-linear connections within the singularity pattern. The asymmetry in swallowtail chaos is less distinguishable in an equilibrated state, but becomes more evident when the system is in a state of non-equilibrium. In many analyses, chaos and catastrophe are examined separately. However, these results demonstrate that when both are present, the two have a complex relationship constrained by the singularity.

Keywords: catastrophe; discrete chaos; non-equilibrium; singular point; Finsler geometry; KCC theory

1. Introduction

Catastrophe, bifurcation, and chaos hold significant importance in both the field of general dynamical systems (e.g., [Thom, 1972; Brown, 1995; Elaydi, 2007]) and concrete systems (e.g., [Rinaldi *et al.*, 1993; Ramu *et al.*, 1994; Nagy & Tasnádi, 2013]). It is widely recognized that the three concepts are mutually interdependent and that both catastrophe and chaos have a complex relationship with bifurcation [Gilmore, 1981; Chen, & Leung, 2012; Kuznetsov *et al.*, 2023]. Consequently, there is a belief that catastrophe and chaos are also intrinsically linked (e.g., [Gilmore, 1981; Gaito & King, 1989; Elaydi, 2003]), although the amount of research in this area is relatively limited compared to bifurcation and chaos (e.g., [Kam, 1992; Qin *et al.*, 2006; Jakimowicz, 2010; Nagy & Tasnádi, 2013; Gu & Chen, 2014]).

Alternatively, Kosambi-Carten-Chern (KCC) theory in Finsler geometry or manifolds [Antonelli, & Bucataru, 2003; Antonelli *et al.*, 2014] has recently been used to study catastrophes (e.g., [Yamasaki & Yajima, 2020, 2022b]), bifurcations (e.g., [Yamasaki & Yajima, 2017; Liu *et al.*, 2021b]) and chaos [Gupta, &

Yadav, 2017; Chen *et al.*, 2020; Liu *et al.*, 2021a; Wei *et al.*, 2022; Munteanu, 2022a; Zhang, 2023]. Hence, it follows that these phenomena will be examined from a unified Finsler geometry perspective. This paper aimed to elucidate the connection between catastrophe and chaos utilizing KCC theory, a geometric theory of bifurcation. Furthermore, this study is focused on a 1D discrete chaos system. Therefore, numerical methods for Lyapunov exponents from the field of discrete mathematics are applied (e.g., [Geist *et al.*, 1990; Lynchi, 2007; Toth *et al.*, 2017; Li *et al.*, 2020]).

In KCC theory, the geometric quantities of Finsler geometry, specifically the non-linear connection and the deviation curvature, have a significant role in stability (e.g., [Sabău, 2005a,b; Harko & Sabău, 2008; Munteanu, 2022b]) and have been applied across various fields such as Newtonian astrophysics [Boehmer & Harko, 2010], the inverse problem on updating parameters of the system[Sulimov *et al.*, 2018], the resonant non-linear Schrödinger system[Lai *et al.*, 2022], the traveling wave solutions of the modified equal width-Burgers wave equation [Liu *et al.*, 2022a], the extended Malkus-Robbins dynamo [Chen *et al.*, 2021], the Navier-Stokes system [Kumar *et al.*, 2019], and the three point vortex field [Hirakui, & Yajima, 2021]. Because the non-linear connection and deviation curvature are already utilized in catastrophe studies [Yamasaki & Yajima, 2020], their diversion to the study of chaos tends to streamline the analysis. However, because deviation curvature, as opposed to the non-linear connection, has been widely adopted as the geometric quantity in chaos analysis (e.g., [Harko *et al.*, 2015; Chen, & Yin, 2019; Huang *et al.*, 2019; Liu *et al.*, 2020; Wang *et al.*, 2021; Liu *et al.*, 2022b]), a discussion of the correlation between non-linear connections N and chaos is needed to begin the analysis.

Therefore, in Section 2, we discuss the relationship between N and chaos, with a focus on one-dimensional (1D) elementary systems, specifically cusp, swallowtail, and butterfly catastrophes, which correspond to 1D discrete chaos, referred to as "chaos" hereinafter. In continuous three-dimensional (3D) systems, the maximal Lyapunov exponent is closely linked to the Jacobi stability through deviation curvature [Oiwa, & Yajima, 2017; Yajima & Nakase, 2021]. On the other hand, it is widely recognized that the Lyapunov exponent L can be used to determine chaos for 1D discrete systems (e.g., [Elaydi, 2007; Ashish *et al.*, 2021]). Thus, this study provides evidence that L is linked to a statistical measure of information concerning N. This study refers to non-linear connections information as N_I, in which N is related to the non-equilibrium stability of the dynamical system [Yamasaki & Yajima, 2013]. Our findings suggest that the magnitude of N_I is useful for chaos determination based on non-equilibrium stability and is a differential geometric representation of the Lyapunov exponents based on the KCC theory.

Section 3 examines the catastrophe cusp as an illustration of N_I-based analysis. The bistability of the catastrophe gives rise to initial value dependence, or hysteresis, in the chaotic pattern. Additionally, there is an abrupt change between chaos and non-chaos. For instance, we will observe a direct shift from node to chaos without cycle stage. In the N_I-valued contour topography, the abrupt change is observed as a cliff (as a line of critical points), whereas the initial dependence is detected as topographic invertibility.

Section 4 of this paper focuses on the impact of deviation curvature P on chaos. In Finsler geometry, P is a geometric quantity of a higher order than N [Antonelli *et al.*, 1993]. Therefore, P statistic effects on chaos can be viewed as corresponding to higher-order "Lyapunovianity". This section discusses the catastrophe butterfly as an illustration to provide clarity regarding the two primary geometric quantities in chaos, namely N and P. Briefly, the statistical analysis of N is linked to chaos determination, and the statistical analysis of P is linked to the degree of chaos development. Both concepts are mathematically connected, therefore, they are interrelated.

Section 5 of this paper explores the non-equilibrium properties of chaos. Previous research has demonstrated the usefulness of N and P in analyzing stability in non-equilibrium regions [Yamasaki & Yajima, 2016, 2022a]. Because chaos is a phenomenon that is typically associated with non-equilibrium, taking this perspective is beneficial for the analysis. To illustrate, this section explores the swallowtail catastrophe. Not only does chaos in the dynamic equilibrium state highlight the chaotic nature of the system after a sufficient amount of time has passed, but chaos in the non-equilibrium state during the process leading up to it also emphasizes its nature.

Section 6 of this paper considers the chaos that arises when two parameters are bivariate. Unlike logistic systems commonly used in chaos studies, the catastrophe systems discussed in this paper possess two or more parameters. Consequently, fixing specific parameters is a common analytical method. However, parameters in nature are typically not constant and may exhibit interdependence. Thus, this study explores the correlation between patterns of chaos and singularity under bivariate conditions. We demonstrate that the size of the chaos-generating region in parameter space is related to the presence or absence of information on non-linear connections within the singularity pattern.

Section 7 of this paper summarizes the key findings in four tables.

2. Method 1: Non-linear connections information, N_I

In this section, we examine the correlation between the Lyapunov exponent utilized in analyzing 1D discrete chaos and the non-linear connection of Finsler geometry. To illustrate this, the logistic system is taken as an example.

2.1. *Brief overview of Kosambi-Carten-Chern theory in catastrophes*

In the examination of 1D discrete chaos, the logistic system is frequently utilized:

$$\dot{n} = bn(1-n), \tag{1}$$

using the quadratic recurrence equation, i.e., the quadratic map is [May, 1974, 1976; Buscarino & Fortuna, 2023]:

$$n_{t+1} = bn_t(1-n_t), \tag{2}$$

where b is a constant. Generally, a 1D dynamical system with $n = n(t)$ is given by

$$\dot{n} = F, \tag{3}$$

where F is a function of n. This paper considers the chaos of the recurrence equation corresponding to Eq. (3):

$$n_{t+1} = F(n_t). \tag{4}$$

The Lyapunov exponent used in this paper (Section 2.2) requires differentiating F by the continuous variable n. In a catastrophe, F on the right side of Eq. (3) has a gradient potential f: $F = -\partial_n f$, where f is a function of n [Thom, 1972; Zeeman, 1977]. In KCC theory, consider the case where n on the left side has time potential x: $n = \dot{x}$ (e.g., [Antonelli, 1985; Antonelli *et al.*, 1993; Yamasaki & Yajima, 2017; Antonalli *et al.*, 2019; Yamasaki & Yajima, 2020; Antonalli *et al.*, 2021; Yamasaki & Yajima, 2022b]). In this case, the basic form in KCC theory is $\ddot{x} + g = \dot{n} + g = 0$, where g is a function of n. To avoid confusion regarding signs, we will summarize the relationships between F in Eq. (3), f in a catastrophe scenario, and g in KCC theory:

$$F = -\partial_n f = -g. \tag{5}$$

The concrete form of f is given by n polynomials for each catastrophe (type of singularity) [Thom, 1972; Zeeman, 1977]. From Eq. (5), this also determines the concrete forms of F and g. g represents the geometric quantities of KCC theory (e.g., [Antonelli, & Bucataru, 2003]):

$$N = \frac{1}{2}\partial_{\dot{x}} g = \frac{1}{2}\partial_n g, \tag{6}$$

$$G = \partial_{\dot{x}} N = \partial_n N, \tag{7}$$

$$P = -Gg + N^2, \tag{8}$$

where N represents the non-linear connections, G is a Berwald connection, and P is the deviation curvature. Since every geometric quantity can eventually be expressed in terms of n alone, the time potential $\dot{x}$ can be regarded as a purely mathematical tool [Yamasaki & Yajima, 2017, 2020]. It can also sometimes have a biological or physical meaning (e.g., [Antonelli, 1985; Yajima *et al.*, 2018; Yamasaki & Yajima, 2022b]).

Non-linear connection N and deviation curvature P have a close relationship with non-equilibrium stability and play important roles in the following analysis of chaos.

2.2. *Lyapunov exponent and N_I*

Our approach uses the Lyapunov exponent computed through the derivative method. From Eqs. (1) and (3), F is given by

$$F = bn(1-n). \tag{9}$$

Differentiating F defines the Lyapunov exponent using the derivative method (e.g., [Elaydi, 2007; Lynchi, 2007]):

$$L = \frac{1}{T+1}\sum_{t=0}^{T} \ln|\partial_n F(n_t)|. \tag{10}$$

When calculating the partial derivative of F with respect to n, the recurrence equation value of $n_{t+1} = bn_t(1-n_t)$ from Eq. (9) is utilized instead of the continuous variable n: $\partial_n F(n_0), \partial_n F(n_1), \cdots, \partial_n F(n_T)$ (e.g., [Elaydi, 2007; Lynchi, 2007]).

In summary, the calculation of L is based on the derivative of F, with $\partial_n F$ being calculated using n_t in the recurrence equation. The function F corresponds to $(-g)$ in Eq. (5), and the non-linear connection in Eq. (6) is obtained from the derivative of g. Hence, Eq. (10) can be rewritten as

$$L = N_I + \ln[2], \tag{11}$$

where N_I represents the non-linear connections information in this paper, defined as

$$N_I = \frac{1}{T+1}\sum_{t=0}^{T} \ln|N(n_t)|. \tag{12}$$

As in the case above, N is calculated using the values of n_t from the recurrence equation: $N(n_0)$, $N(n_1)$, $\cdots$, and $N(n_T)$. Equation (11) includes $\ln[2]$, because it is multiplied by a factor of 1/2 from Eq. (6). The statistical condition for chaos satisfies $L > 0$ (e.g., [Elaydi, 2007; Lynchi, 2007]), which gives us the corresponding condition for N_I based on Eq. (11):

$$N_I > -\ln[2] \approx -0.693147\cdots. \tag{13}$$

Let us evaluate this using the logistic system. Based on Eq. (9), the non-linear connection can be determined from Eqs. (5) and (6), as given by

$$N_{\text{Logistic}} = -\frac{b(1-2n)}{2}. \tag{14}$$

Substituting Eq. (14) into Eq. (12) yields the following expression:

$$N_I = \frac{1}{T+1}\sum_{t=0}^{T} \ln\left|-\frac{b(1-2n_t)}{2}\right|, \tag{15}$$

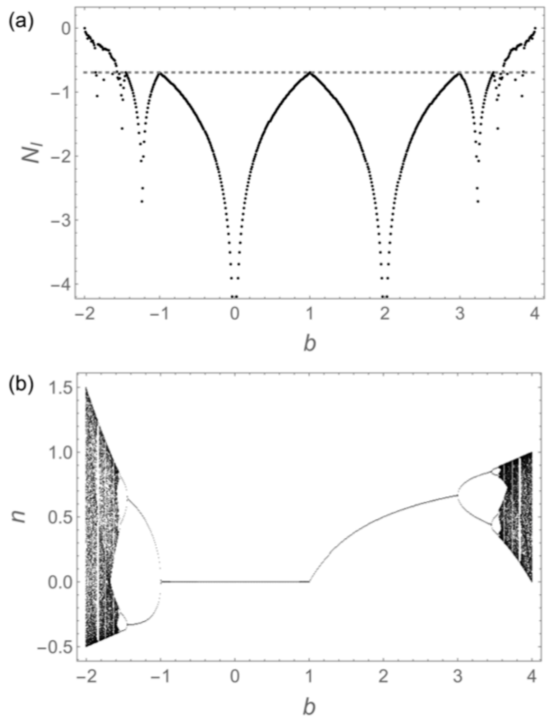

Fig. 1. (a) Logistic's N_I ($T = 10^5$, $n_0 = 0.01$). Gray dotted line is the critical value: $-\ln[2] \approx -0.693\cdots$. (b) Corresponding bifurcation diagram.

where n_t is given by $n_{t+1} = bn_t(1 - n_t)$ from Eq. (9). The results of the calculation for N_I are presented in Fig. 1(a); Fig. 1(b) shows the corresponding bifurcation diagram. From a comparison of the two figures, bifurcation takes place at $N_I = -\ln[2]$ and the onset of chaos occurs when $N_I > -\ln[2]$. The b value in every case is also consistent with the previous analysis (e.g., [Elaydi, 2007; Lynchi, 2007]).

The detailed method for calculating N_I in Fig. 1(a) is presented below. For a more detailed mathematical discussion and background on the iteration and derivative methods used, please refer to the following references: [Geist *et al.*, 1990; Lynchi, 2007; Toth *et al.*, 2017; Li *et al.*, 2020]. From the terms in Eq. (15): $\ln|-b(1-2n_t)/2|$ and $n_{t+1} = bn_t(1-n_t)$, for $t = 1$ we have

$$\ln\left|-\frac{b(1-2n_1)}{2}\right| = \ln\left|-\frac{b(1-2bn_0(1-n_0))}{2}\right|. \tag{16}$$

Thus, by fixing the value of b as b_f, we can estimate the value at $t = 1$ in Eq. (15) from the initial value n_0:

$$\ln\left|-\frac{b_f(1-2b_f n_0(1-n_0))}{2}\right| = \ln\left|-\frac{b_f(1-2F(n_0))}{2}\right|, \tag{17}$$

where $F(n_0) = b_f n_0(1-n_0)$. Through iteration, it is possible to estimate the value from the initial value n_0, even when $t = 2$:

$$\ln\left|-\frac{b_f(1-2n_2)}{2}\right| = \ln\left|-\frac{b_f(1-2F(n_1))}{2}\right| \\ = \ln\left|-\frac{b_f(1-2F(F(n_0)))}{2}\right| \\ = \ln\left|-\frac{b_f(1-2F^2(n_0))}{2}\right|. \tag{18}$$

For any given value of t, we obtain

$$\ln\left|-\frac{b(1-2n_t)}{2}\right| = \ln\left|-\frac{b_f(1-2F^t(n_0))}{2}\right|. \tag{19}$$

Once the initial values are determined, we can compute values from $t = 0$ to $t = T = 10^5$. Therefore, by computing the sum of Eq. (15) and dividing it by $T+1$, a single point in $b = b_f$ can be obtained, as shown in Figure 1(a). Next, by shifting the value of b_f by 0.01 and repeating the same calculation, N_I can be estimated for various b_f as shown in Figure 1(a).

A sufficiently large value of T is considered to be statistically significant (e.g., [Lynchi, 2007]), and therefore $T = 10^5$ is used in this study. The fixed value of b has a shift interval of 0.01, which is deemed sufficient, because the main focus of this study is the analysis of the global pattern of the bifurcation diagram, rather than the local pattern, such as the window in chaos.

As shown below, this study calculates N_I in the Cusp, Butterfly, and Swallowtail cases. In each singular case, the functional form of the Eq. (19) containing $F^t(n_0)$ is replaced by the appropriate one. In this case, Eq. (19), which is linear with respect to n_t, becomes non-linear with respect to n_t; however, the calculation technique is the same.

Additionally, statistics for deviation curvature are also calculated, and the functional form of N_I replaces that of deviation curvature. If the number of parameters increases to two, the calculation is first carried out with both values fixed. Then, each value is calculated by shifting them as described above.

N_I, similar to L, can be used to identify chaos. To calculate N_I, we utilized N, a non-linear connection that contains information about non-equilibrium stability and whose sign determines the type of N-stability [Yamasaki & Yajima, 2013, 2016]. Hence, the identification of chaos through N_I considers non-equilibrium stability, specifically the presence of chaos resulting from changes in the magnitude of N-stability. That is, since Eq. (12) calculates the absolute values of N, if the stability magnitude exceeds a critical value, the system becomes chaotic, regardless of whether the system is N-stable or N-unstable.

Finsler geometry includes geometric quantities of a higher order in the form of deviation curvature P and, its corresponding concept, J-stability [Antonelli, & Bucataru, 2003; Sabău, 2005a,b], expanding on that of non-linear connections. This allows for the exploration of higher-order Lyapunovianity through Finsler geometry, as described in Section 4.

Non-linear connections and deviation curvature have both been derived specifically for catastrophes [Yamasaki & Yajima, 2020, 2022b]. This allows for the direct conversion to chaos analysis for each type of catastrophe: cusp, butterfly, and swallowtail. The next section will focus on the cusp specifically.

3. Chaos in cusp

3.1. *Geometric quantities and singular pattern*

This section considers chaos in cusp. In Eq. (3), F is [Thom, 1972; Zeeman, 1977]

$$F_{\text{cusp}} = -\partial_n f_{\text{cusp}} = -(n^3 + an + b), \tag{20}$$

where a, b are constants. Thus, from Eq. (5),

$$g_{\text{cusp}} = n^3 + an + b. \tag{21}$$

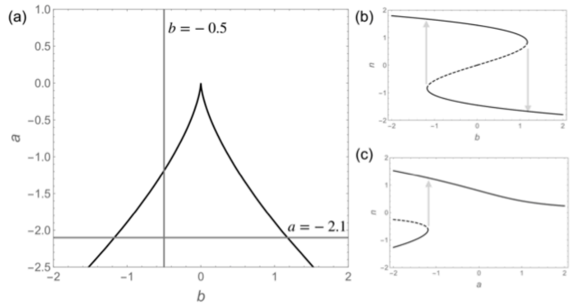

Fig. 2. (a) Cusp singularity. (b) Equilibrium solutions for $a = -2.1$. (c) Equilibrium solution for $b = -0.5$. In both (b) and (c), the solid line is stable, the dotted line is unstable, and the gray arrow is a catastrophe.

We have demonstrated the derivation of the subsequent geometric parameters [Yamasaki & Yajima, 2020]:

$$N_{\text{cusp}} = \frac{1}{2}(3n^2 + a), \tag{22}$$

$$P_{\text{cusp}} = \frac{1}{4}(-3n^4 - 6an^2 - 12bn + a^2). \tag{23}$$

From the equilibrium condition $g_{\text{cusp}} = 0$ and the neutral N-stability $N_{\text{cusp}} = 0$, the singular pattern in the equilibrium state can be obtained [Yamasaki & Yajima, 2022b]. Figure 2(a) is well known and can be derived from Eqs. (21) and (22). The logistic system has only one parameter b (Eq. (9)); however, cusp has two parameters a, b (Eq. (20)). Therefore, we fix one of them to investigate chaos behavior. Figures 2(b) and (c) illustrate the equilibrium solutions from $g_{\text{cusp}} = 0$ with fixed parameters. The stable (unstable) equilibrium solutions are represented by a solid (dotted) line, resulting in a catastrophic outcome, as indicated by an arrow.

3.2. *Chaos with fixed a*

The computation method for determining the non-linear connections information, N_I, is identical to that of the logistic case. This involves substituting Eq. (22) into Eq. (12):

$$N_I = \frac{1}{T+1}\sum_{t=0}^{T} \ln\left|\frac{1}{2}(3n_t^2 + a)\right|. \tag{24}$$

To calculate n_t, from Eq. (20), we use

$$n_{t+1} = -(n_t^3 + an_t + b). \tag{25}$$

The distinction from the logistic instance is that the cusp is concomitant with a catastrophe, as displayed by the arrows in Figs. 2(b) and (c). Because the N value may vary rapidly, the value of N_I can also change rapidly. As a consequence, chaos can occur discontinuously, rather than continuously as in logistics. This chaos exhibits an additional feature of catastrophes: initial dependence (hysteresis). As illustrated in Fig. 2(b), when the absolute value of the initial value is identical, but the sign varies, the catastrophe's occurrence location is reversed. This means that the system is a multi-stable type. The chaotic pattern further demonstrates this.

As an example, let's consider the case where $a = -2.1$. The initial values are $n_0 = \pm 0.3$, and we can see the resulting N_I and n calculated from Eqs. (24) and (25), as shown in Fig. 3. Similar to the logistic case (Fig. 1), bifurcation occurs at $N_I = -\ln[2]$ and chaos occurs when $N_I > -\ln[2]$. However, this case differs from the logistic case, as N_I changes suddenly (almost discontinuously). Thus, there is a point where the

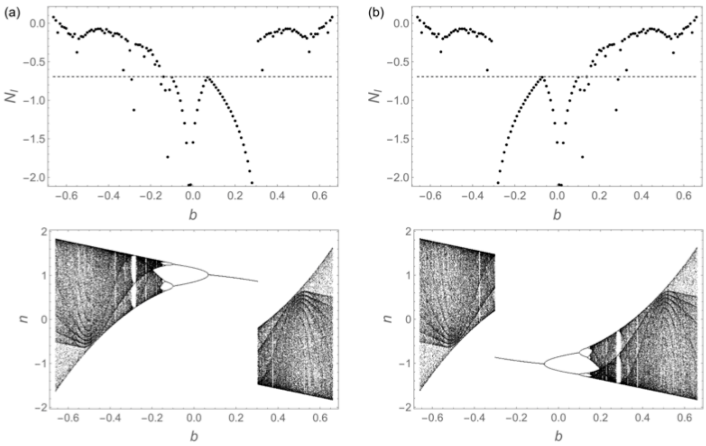

Fig. 3. Cusp's N_I ($a = -2.1$, $T = 10^5$) and corresponding bifurcation diagram for (a)$n_0 = 0.3$ and (b)$n_0 = -0.3$.

transition between non-chaotic and chaotic is abrupt. Unlike the catastrophe from one equilibrium solution to another, as depicted in Fig. 2(b), this sudden chaotic transition transpires within the non-equilibrium state. Although this explanation is qualitatively correct, this sudden transition seems to be closely related to catastrophes in dynamical systems. Therefore, additional quantitative studies from this perspective are required. Section 3.3 shows quantitatively that the location of critical values in a catastrophe constrains the location of abrupt transitions in chaos. Additionally, the position of the critical value for unstable equilibrium solutions is related to the multi-stability of chaos. Therefore, the abrupt transition of chaos reflects the nature of the catastrophe phenomenon, albeit in a non-equilibrium regime.

Furthermore, opposite signs in Figs. 3(a) ($n_0 = 0.3$) and 3(b) ($n_0 = -0.3$) yield opposite patterns. Specifically, upper and lower patterns develop, as shown in Figs. 3(a) and (b), respectively. The initial criticality of the upper and lower patterns was determined by the positional relationship with respect to the non-equilibrium stability. This feature will be analyzed further in the following section.

The above examples represent a case where $n_0 = \pm 0.3$ and $a = -2.1$. These results are applicable to other cases where n_0 varies from ± 0.01 to ± 1.7. Additional results beyond $a = -2.1$ are addressed in Section 3.5.

Catastrophe theory suggests that when the control parameter (cause) changes continuously, the corresponding outcome changes discontinuously. Chaos theory suggests that the type of trajectory changes qualitatively from stationary or periodic to chaotic with a continuous change in the control parameter. As shown in Fig. 3 of the present study, both of these phenomena can occur simultaneously.

As a physical example, it has been noted that continuous changes in the solar constant can cause catastrophic changes in climate (e.g., [Ghil, & Childress, 1987; Eisenman, & Wettlaufer, 2009; Bathiany *et al.*, 2018]). Additionally, the climate may be changing chaotically (e.g., [Shukla, 1998; Lenton *et al.*, 2008; Pisarchik, & Feudel, 2014]). Although the climate change phenomenon is more complex than the models analyzed in this study, the results suggest that catastrophe and chaos can occur simultaneously even in the simplest case.

The following sections will demonstrate the complexity of the relationship between the two and how it is influenced by the singularity's nature.

3.3. *Critical point in catastrophe's chaos*

To analyze the dependence of chaos patterns on initial values, we examine the development process of the bifurcation diagram. For this analysis, here we apply the critical point determined by the initial value, represented as $n_{t+1} = n_t = \cdots = n_0$ (e.g., [Elaydi, 2007; Lynchi, 2007]). In the (b, n_t) space bifurcation diagram, the critical point's location restricts the location and pattern of sudden changes in the space.

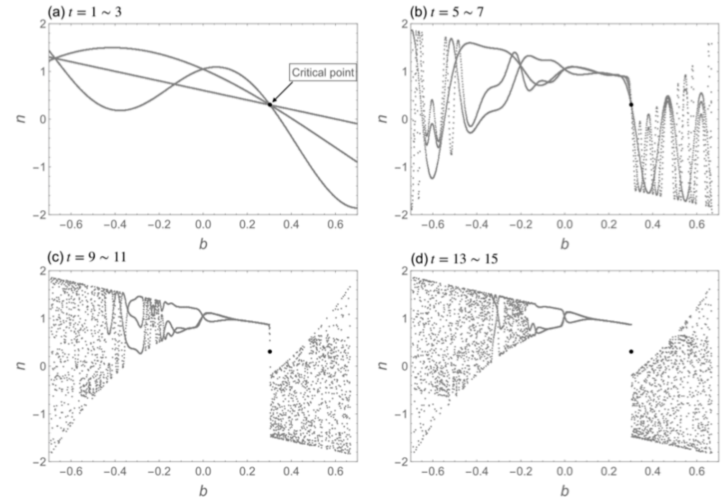

Fig. 4. Bifurcation diagram for each t period under the same conditions as Fig. 3. The black dot is a critical point.

As an example, Fig. 4 presents the bifurcation diagram for each time period t under the same conditions as Fig. 3(a): $a = -2.1$ and $n_0 = 0.3$. The depiction for $t = 1 \sim 3$ superimposes the values of n_1, n_2, and n_3 for each parameter b, resulting in three curves (Fig. 4(a)). As the interval for t is 3 during all periods, the perceived presence of numerous chaos points is, in fact, an illusion (Figs. 4(c)(d)). The point where all trajectories intersect, the so-called critical point, is observed. As t increases, an abrupt shift occurs in the b-coordinate of the critical point.

Next, we will determine the coordinates of the critical point in the general case. Let (b_0, n_0) denote the coordinates of a critical point in (b, n) space as depicted in Fig. 4. In the case of a cusp, $n_{t+1} = -(n_t^3 + an_t + b)$ and $n_{t+1} = n_t = \cdots = n_0$ result in

$$b_0 = -n_0(n_0^2 + a + 1). \tag{26}$$

Given a fixed value of a, the coordinates (b_0, n_0) of the critical point can be determined by providing an initial value of n_0. The stability of the non-equilibrium region holds significant importance in this case and, hence, we calculate the KCC stability using Eqs. (22) and (23). According to [Yamasaki & Yajima, 2017], the system is N-stable (-unstable) when N is positive (negative). Moreover, the system is J-unstable (-stable) when P is positive (negative). Further details on each stability are provided in [Yamasaki & Yajima, 2020] (see also [Munteanu *et al.*, 2023a; Munteanu, 2023b] for higher dimensions). For the sake of convenience, the combinations of N-stability and J-stability are unified in grayscale:

- J-stable $P < 0$ and N-stable $N > 0$: light gray
- J-stable $P < 0$ and N-unstable $N < 0$: white
- J-unstable $P > 0$ and N-stable $N > 0$: dark gray
- J-unstable $P > 0$ and N-unstable $N < 0$: black

It has been demonstrated that a system located in the black or white region transitions to a nearby light or dark gray region (e.g., [Yamasaki & Yajima, 2017]). To clarify this in more typical terms, referring to Fig. 2(b), if the initial value is above the unstable equilibrium solution (center dotted line), then the transition occurs to the upper stable equilibrium solution (upper solid line). Likewise, if the initial value is below the dotted line, the transition is to the stable equilibrium solution situated underneath. Thus, if the value of n_0 at the critical point (26) exceeds the unstable solution, the upper bifurcation diagram will develop, and if it is lower, so will the lower bifurcation diagram. The unstable solution in the cusp: n_{us}, derived by Yamasaki & Yajima (2020), is reformulated in terms of b_0 in Eq. (26):

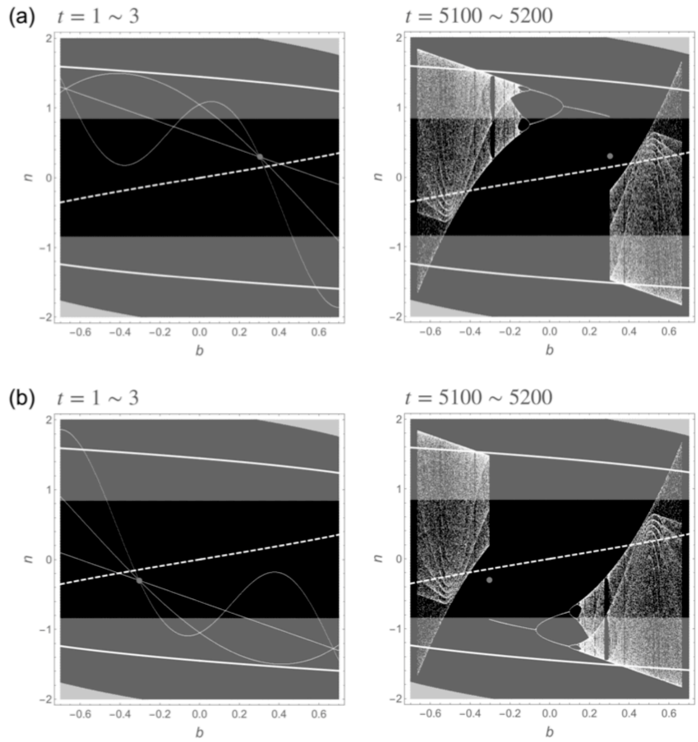

Fig. 5. Stability and bifurcation diagram superimposed under the same conditions as Fig. 3. (a)$n_0 = 0.3$. (b)$n_0 = -0.3$. The round gray point is a critical point calculated from Eq. (27). The white lines are equilibrium solutions (solid is stable and dotted is unstable). Non-equilibrium stability is gray scaled (see main text).

$$n_{\mathrm{us}} = \frac{2^{2/3}\sqrt[3]{3}\left(-1 - i\sqrt{3}\right)\left(\sqrt{12a^3 + A^2} + A\right)^{2/3} + 2\sqrt[3]{2}\sqrt[6]{3}\left(\sqrt{3} - 3i\right)a}{12\sqrt[3]{\sqrt{12a^3 + A^2} + A}}, \tag{27}$$

where $A = 9n_0\left(a + n_0^2 + 1\right)$.

For instance, Fig. 5 examines identical conditions to those used in Fig. 3: $a = -2.1$ and the initial value of $n_0 = \pm 0.3$. The critical point (b_0, n_0) is computed from Eq. (26), resulting in the round gray point. If the critical point of the black region is proximate to the dark gray region above, then the upper bifurcation diagram will develop. Conversely, if it is below, the lower diagram will develop. Specifically, when $a = -2.1$ and $n_0 = \pm 0.3$, Eq. (27) yields $n_{\mathrm{us}} \approx \pm 0.146$ (the same sign order), i.e., n_0 is above (below) n_{us}, respectively.

The same pattern can be replicated with alternative initial values. The following is a supplement. For instance, when $a = -2.1$, as described above, the range for b in which the unstable equilibrium solution n_{us} exists is $-1.17 < b < 1.17$ (refer to Fig. 2(b)). It should be noted that b_0 in Eq. (26) may exceed this range, relying on the initial values selected. In this case, instead of using the coordinates (b_0, n_0) of the critical point for $t \geq 0$ as mentioned above, we should utilize the coordinates (b_1, n_1) of the critical point that exists for $t \geq 1$. In this case, b_1 represents the situation where $n_{t+1} = n_t$, but the initial value is one mapping of $-(n_0^3 + an_0 + b)$, and not n_0:

$$b_1 = 0.5\left(\pm\sqrt{-4a - 3n_0^2} - 2an_0 - 2n_0^3 + n_0\right). \tag{28}$$

For instance, the initial value $n_0 = 1.5$ is larger than $n_0 = -1.5$. However, according to Eq. (28) and within

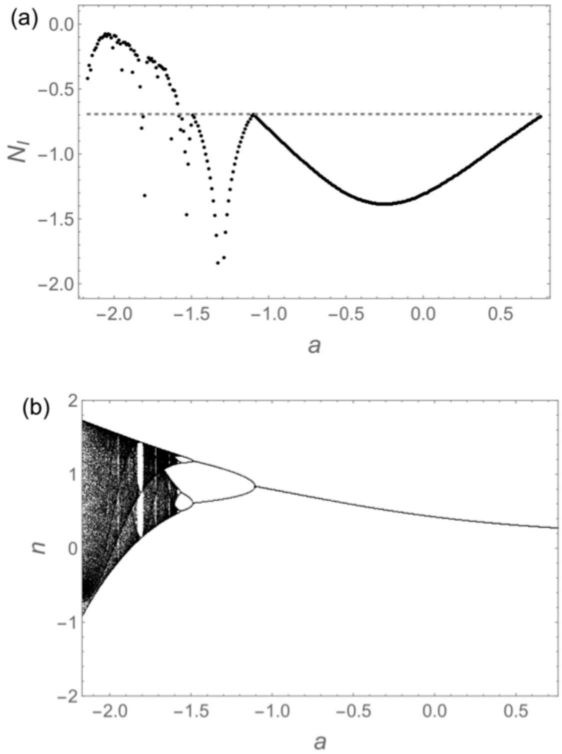

Fig. 6. (a) Cusp's N_I. (b) Corresponding bifurcation diagram. $b = -0.5$, $T = 10^5$, and $n_0 = 0.3$.

the range of $-1.17 < b < 1.17$, where unstable solutions exist, $n_1|_{n_0=\pm1.5} \approx \mp 0.108$, resulting in a reversal of the large/small relationship. As a result, a lower pattern develops when $n_0 = 1.5$, while an upper pattern occurs when $n_0 = -1.5$.

3.4. *Chaos with fixed b*

In this section, we examine chaos when the parameter b is held constant. We use the same analytical approach as in the previous section, but interchange the roles of parameters a and b. Initially, N_I is calculated utilizing Eqs. (24) and (25), with b fixed and an initial value of n_0 given. Subsequently, a is varied. As an example, Fig. 6 shows the results of the analysis when $b = -0.5, n_0 = 0.3$. As implied by Fig. 2(c), an asymmetric pattern emerges. The case of other n_0 and b values is presented in the following section, together with changes in a.

3.5. *N_I in parameter space*

In the previous analysis, one parameter of the two, namely a or b, was kept fixed, while N_I was computed. For the purpose of visual clarity, this section presents the distribution of $N_I + \ln[2]$ over (a, b) space, rather than just N_I itself. Accordingly, positive regions correspond to chaotic behavior, while negative regions indicate non-chaotic behavior. The calculation for N_I remains based on Eqs. (24) and (25), as earlier. However, the parameters a and b are now not fixed, resulting in a two-dimensional (2D) contour plot of $N_I + \ln[2]$. Since both parameters, a and b, are varied, the following 2D plot displays a more comprehensive view of the two significant features: (1) a sudden, catastrophic shift in mode and (2) initial dependence (hysteresis).

As an example, we consider the case with the initial condition of $n_0 = 0.3$, as shown in Fig. 7(a). The cross-section of $a = -2.1$ corresponds to Fig. 3(a). The cross-section of $b = -0.5$ corresponds to Fig. 6. In Fig. 7(b), where $n_0 = -0.3$ (the sign changes), the pattern is inverted. This figure displays the

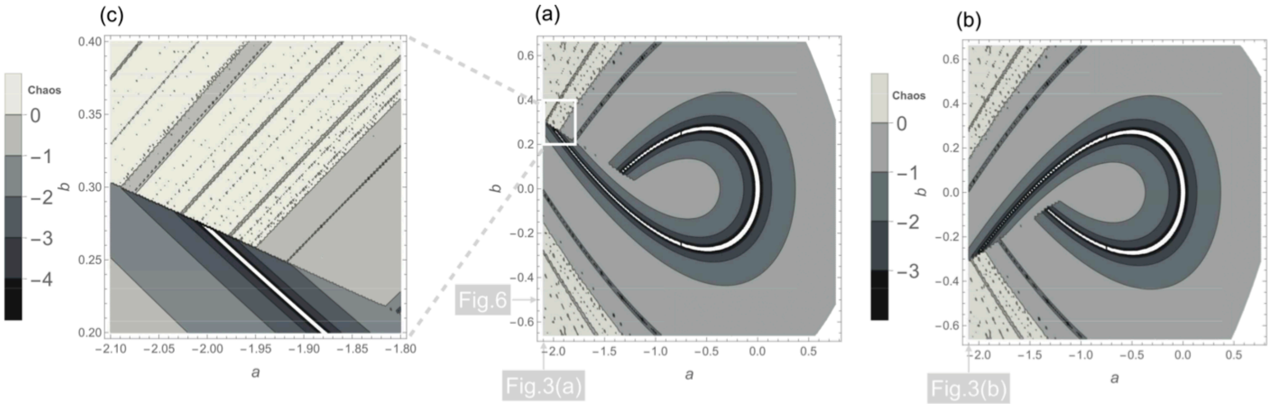

Fig. 7. Contour topography of $(N_I + \log 2)$-values in parameter space for (a) $n_0 = 0.3$ and (b) $n_0 = -0.3$. (c) Enlarged view of the white rectangle area in (a). Positive area is chaos.

impact of initial dependence, as previously discussed. One of these cross-sections is depicted in Fig. 3(b). An enlarged image of the white rectangle area in Fig. 7(a) is depicted in Fig. 7(c). The abrupt alteration in the boundary solidifies the distinction between the negative region (non-chaotic) and the positive region (chaotic). Due to the presence of this cliff-like, discontinuous boundary, the transition from non-chaotic to chaotic is characterized as being similar to a catastrophe. The cross-sectional examples of this are the catastrophes depicted in Figs. 5(a) and 5(b). The existence of the linear set of critical points is responsible for the cliff formation.

In 1D discrete systems, calculations may diverge to infinity if the parameter values are sufficiently large ([Hirsch *et al.*, 2012]). Furthermore, the results diverge technically in a range well beyond the minimum indicated by the contour lines (e.g., -5 in Figure 7(c)). In this paper, these parameter ranges are represented as pure white in the contour topography. This also applies to other contour topographies.

When both parameters are varied, the contour pattern depends only on the initial value. As shown above, changing the sign of the initial value reverses the pattern. Next, let us consider the effect of the magnitude of the initial value. To simplify, assume $n_0 = n$ in the formula $n_{n+1} = -(n_t^3 + an_t + b)$ and focus solely on the constant terms (terms unrelated to n) after mapping three times:

$$C = b\left((3-3a)b^6 - 3(1-a)^2b^4 + (a((3-a)a-4)+1)b^2 + (1-a)a - b^8 - 1\right). \tag{29}$$

From Eq. (22), plotting $\ln|N_c|$ with $N_c = (1/2)(3C^2+a)$ results in a pattern resembling a heart shape, owing to its polynomial characteristics. As the mapping is repeated more frequently, the heart shape becomes more pronounced. The pattern depicted in Fig. 7 is the average obtained from each mapping, according to the sum in Eq. (24). The constant term produces the heart-shaped pattern, while the non-constant term that relies on the initial value modifies it.

For instance, when the initial value is small (e.g., $n_0 = 0.01$), a closed heart shape emerges, as depicted in Fig. 8(a). If the initial value increases (e.g., $n_0 = 0.1$), the bias of the critical point results in a dislocation in the heart-shaped structure (Fig. 8(b)). This dislocation progresses with the magnitude of the initial value, leading to the formation of a cliff at the tip, which displays catastrophic abrupt changes between chaotic and non-chaotic regions (Fig. 7).

4. Method 2: Mean deviation curvature $\overline{P}$

Up to this point, we have examined primarily the impact of non-linear connections N on chaos. However, the KCC theory suggests that deviation curvature P- an essential geometric quantity - is linked to trajectory robustness (e.g., [Dănilă *et al.*, 2016; Harko *et al.*, 2016; Lake & Harko, 2016]). Thus, our analysis of chaos considers the robustness of trajectories based on the deviation curvature.

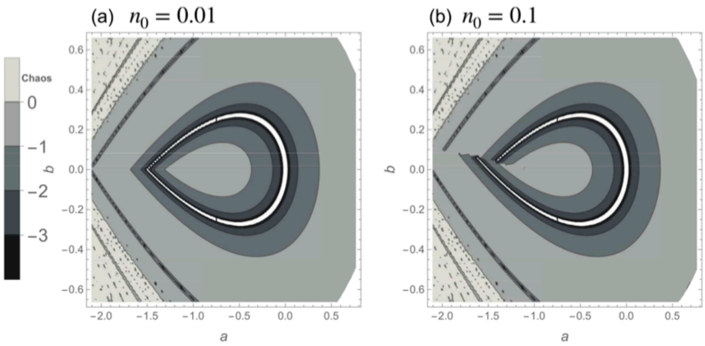

Fig. 8. Contour topography of $(N_I + \log 2)$-values in parameter space for (a)$n_0 = 0.01$, (b)$n_0 = 0.1$.

4.1. *N_I in butterfly*

Our examination focuses on the butterfly (hereinafter, BT), which is a higher-order catastrophe than the cusp. In Eq. (3), F is [Thom, 1972; Zeeman, 1977]

$$F_{\mathrm{BT}} = -\partial_n f_{\mathrm{BT}} = -(n^5 + an^3 + bn^2 + cn + d), \tag{30}$$

where a, b, c, d are constants. Thus, from Eq. (5),

$$g_{\mathrm{BT}} = n^5 + an^3 + bn^2 + cn + d. \tag{31}$$

We have already presented the following geometric quantities [Yamasaki & Yajima, 2020]:

$$N_{\mathrm{BT}} = \frac{1}{2}(5n^4 + 3an^2 + 2bn + c), \tag{32}$$

$$P_{\mathrm{BT}} = \frac{1}{4}\left(5n^4 + 3an^2 + 2bn + c\right)^2 - \left(10n^3 + 3an + b\right)\left(n^5 + an^3 + bn^2 + cn + d\right). \tag{33}$$

The conditions where $g_{\mathrm{BT}} = N_{\mathrm{BT}} = 0$ results in a singular pattern of BT in the equilibrium state [Yamasaki & Yajima, 2022b]. Figure 9 illustrates the outcome of the calculation with the parameter $a = -1.5$. To simplify, we set the bias parameter b [Bröcker, & Lander, 1975] to be zero in this paper. Based on the shape of the singularity pattern, we considered six distinct cases in which parameters c and d cross the pattern. The equilibrium solutions for each case and the results of the KCC analysis for non-equilibrium stability based on Eqs. (32) and (33) are also presented in Fig. 9.

First, as in the cusp case, the analysis was conducted using non-linear connections information, leading to the subsequent analysis based on deviation curvature. The analytical approach is identical to that used for a cusp. Initially, to compute the non-linear connections information N_I for BT, we substitute Eq. (32) into Eq. (12):

$$N_I = \frac{1}{T+1}\sum_{t=0}^{T} \ln\left|\frac{1}{2}(5n_t^4 + 3an_t^2 + 2bn_t + c)\right|. \tag{34}$$

To calculate n_t, from Eq. (30), we use

$$n_{t+1} = -(n_t^5 + an_t^3 + bn_t^2 + cn_t + d). \tag{35}$$

The distribution of N_I within the parameter space plays a pivotal role in determining chaotic behavior, as demonstrated for the cusp. The polynomial Eq. (34) with $b = 0$ indicates that a small initial value results in

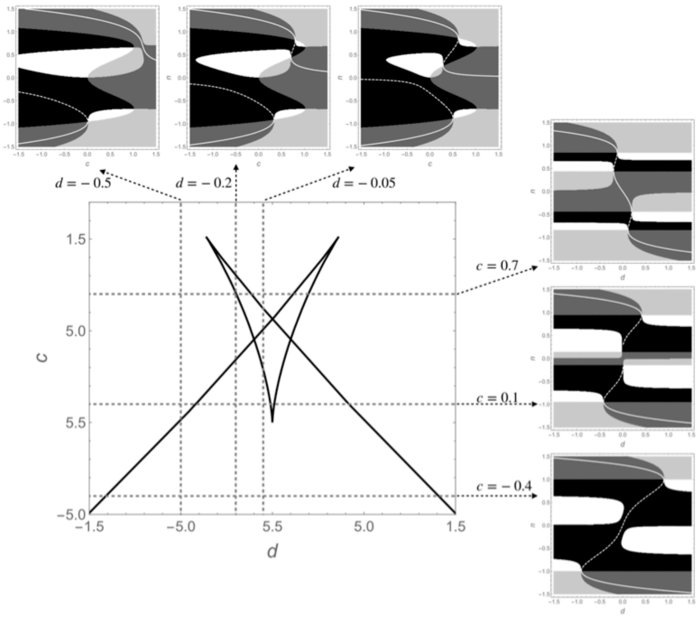

Fig. 9. Butterfly (BT) singularity ($a = -1.5$, $b = 0$). Equilibrium solution (solid is stable and dotted is unstable) and non-equilibrium stability (gray scale, see main text in Section 3.3) for each parameter are also listed.

a heart-shaped distribution, as shown in Fig. 8. If the initial value's magnitude is significant, then left-right asymmetry becomes dominant. If the sign of the initial value changes, the distribution pattern will invert.

Figure 10 shows the distribution of $N_I + \ln[2]$, which was obtained by applying Eqs. (34) and (35) with $a = -1.5$ and an initial value of $n_0 = 0.1$. Also presented in the figure is a bifurcation diagram for each parameter, as shown in Fig. 9. Various combinations of the initial value and a are presented in Fig. 11. Similar to the cusp, Fig. 11(a) illustrates that the heart shape becomes distorted and eventually develops a discontinuity as a increases. Also similar to the cusp, Fig. 11(b) shows that, when the initial value's sign changes, the pattern reverses, and left-right asymmetry prevails with an increase in the initial value's magnitude.

4.2. $\overline{P}$ *in butterfly*

We shall now examine the correlation between deviation curvature P and chaos. Obviously, N and P are not independent, but are associated through Eq. (8), as follows:

$$N^2 = P + Gg. \tag{36}$$

From this equation and Eq. (12), it is evident that the calculation of N_I corresponds to calculations of P and Gg, but it does not account for the net effect of P alone. The relevance of N_I in determining chaos implies that it is challenging to make a chaos determination based solely on the calculation of P. As a consequence, previous chaos analyses that depended primarily on P proved to be valuable, but were complicated by the existence of G and g. If N is large enough to be prone to chaos, the sign of P can be determined from $P = N^2 - Gg \approx N^2 > 0$. However, it remains unclear as to how the magnitude of P affects chaos.

Therefore, here we take a closer look at the net effect of $P's$ magnitude on chaos. Defining a corresponding P statistic, such as N_I for N, is desirable. The time average of P is the simplest statistic to consider:

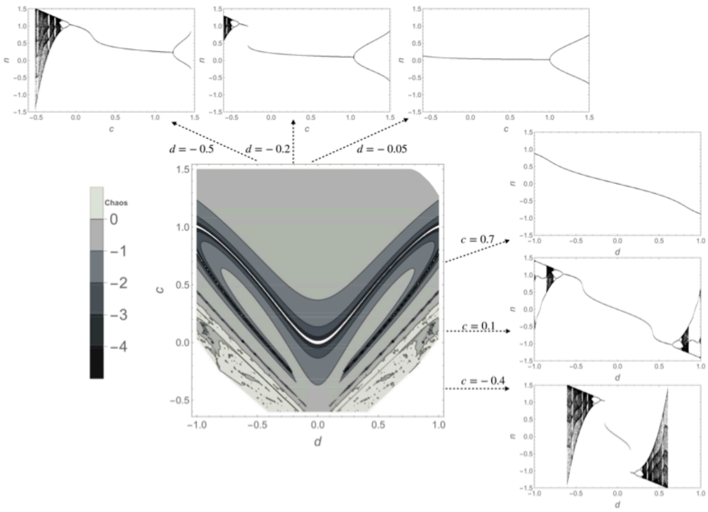

Fig. 10. Contour topography of $(N_I + \log 2)$-values in parameter space of BT. $n_0 = 0.01$ and other conditions are the same as in Fig. 9. The positive area is chaotic, and the corresponding bifurcation diagrams are also listed.

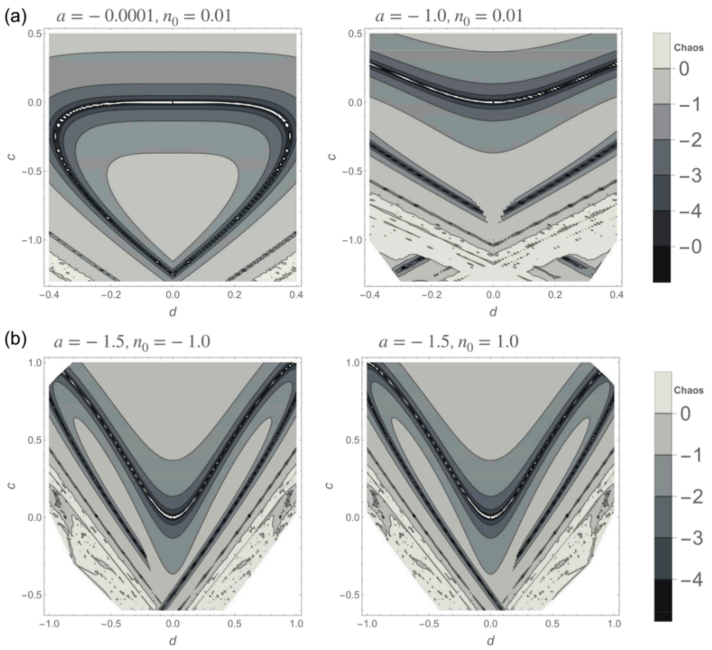

Fig. 11. Contour topography of $(N_I + \log 2)$-values in parameter space of BT. (a) Fix initial value as $n_0 = 0.01$ and change parameters: $a = -0.0001$ and $a = -1$. (b) Fix the parameter as $a = -1.5$ and change the initial values: $n_0 = -1.0$ and $n_0 = 1.0$.

$$\overline{P} = \frac{1}{T+1} \sum_{t=0}^{T} P(n_t). \tag{37}$$

In this paper, this statistic is referred to as the mean deviation curvature.

Previous research has demonstrated a correlation between P and the robustness of the trajectory, and has concentrated primarily on the sign of P (e.g., [Dănilă *et al.*, 2016; Harko *et al.*, 2016; Lake & Harko, 2016]). Further research has revealed that the magnitude of P is linked to the level of robustness described by the Douglas tensor (e.g., [Antonelli, & Bucataru, 2003; Yamasaki & Yajima, 2020, 2022b; Munteanu, 2023b]). For instance, as the value of P increases (decreases), the robustness of the trajectory will decrease (increase), resulting in a more localized (globalized) trajectory. However, the role of the statistic $\overline{P}$ in chaotic systems remains unclear. Thus, we initiate our analysis by calculating $\overline{P}$ for the chaos case and observing its correlation with the chaos trajectory.

As a simple example, consider a situation in which only chaos develops. Chaotic regions on both sides of the parameter space (Fig. 11) merge at the tip as c decreases. For consistency with Fig. 11, we calculate $N_I + \ln[2]$ under identical conditions: $a = -1$, $b = 0$ and $n_0 = 0.01$, utilizing Eqs. (34) and (35). Figure 12(a) expands the merging area. The bifurcation diagram is presented in Fig. 12(b), computed for $c = -1.33$, illustrating the merger of the chaos on both sides. Because the chaos on both sides ($d < -0.04$ and $d > 0.04$) and in the merging region ($-0.04 < d < 0.04$) have differing oscillation widths, we refer to the former as (relatively) local chaos and the latter as (relatively) global chaos in this paper.

Figure 12(c) displays the computed value of N_I that corresponds to Fig. 12(b) using Eqs. (34) and (35). As it is chaotic throughout almost all regions, most of the values surpass the critical value: ($-\ln[2]$) (represented by the dotted line). The variation is insignificant, only marginally differentiating at the boundaries of the merging region, while presenting gently mountainous patterns for both local chaos ($d < -0.04$ and $d > 0.04$) and global chaos ($-0.04 < d < 0.04$).

Finally, we compute $\overline{P}$ corresponding to Fig. 12(b) by substituting Eq. (33) into Eq. (37):

$$\overline{P} = \frac{1}{T+1}\sum_{t=0}^{T}\left(\frac{1}{4}\left(5n_t^4 + 3an_t^2 + 2bn_t + c\right)^2 - \left(10n_t^3 + 3an_t + b\right)\left(n_t^5 + an_t^3 + bn_t^2 + cn_t + d\right)\right). \tag{38}$$

To calculate n_t, use Eq. (35): $n_{t+1} = -(n_t^5 + an_t^3 + bn_t^2 + cn_t + d)$. The results of the computation are presented in Fig. 12(d), indicating that $\overline{P}$ is positive across all regions. The degree of robustness differs between global and local chaotic regions, with distinct variations in $\overline{P}$ magnitude and its rate of change. Specifically, the merging region $-0.04 < d < 0.04$ (classified as a global chaotic region) has considerably lower and stable $\overline{P}$ values, indicating a stronger robustness of the trajectory in the region. On the other hand, in regions where $d < -0.04$ or $d > 0.04$ (classified as a local chaotic region), the value of $\overline{P}$ increases, indicating a relatively weak robustness and a more localized trajectory.

These findings suggest that, while non-linear connections provide valuable information for determining chaos, they cannot alone define the characteristics of a chaotic trajectory, which requires the use of deviation curvature statistics. Note that these results are based on a specific case where only chaos exists. In the next section, we will apply the same analysis to the standard examples of BT depicted in Fig. 10, as well as to the cusp shown in Fig. 3(a).

4.3. *Other examples*

In this section, we validate the outcome of the previous subsection: when $\overline{P}$ increases (decreases), the chaotic trajectory becomes localized (globalized). For this, we use two examples of BT chaos in Fig. 10: $c = -0.4$ and $d = -0.5$. Furthermore, we will examine why the density of points at the edges of the left and right regions of chaos are lower in the bifurcation diagram of the cusp displayed in Fig. 3(a).

First, consider Fig. 13(a). The left and right sides are symmetrical as c is fixed and d varies, as depicted in Fig. 10. Calculation for N_I is based on Eq. (34) with (35); $\overline{P}$ is based on Eq. (38) with (35), with the same calculation conditions as in Fig. 10. Chaotic regions, where N_I-values exceed the critical value ($-\ln[2]$), are $d < -0.3$ and $d > 0.3$, and in these areas, little variation is observed. $\overline{P}$-values decrease as d increases for $d > 0$ and decrease with d for $d < 0$. As a result, chaos is anticipated to shift from local to global, with the width of the chaotic region expanding on both sides. This aligns with the bifurcation diagram's trend.

Next, we examine Fig. 13(b), using the same calculation method as in Fig. 12. Because d is held constant and c is adjusted, the left and right sides become asymmetrical (Fig. 10). In the chaotic region ($c < -0.19$), N_I values surpass the critical value ($-\ln[2]$) and little variation is observed, while $\overline{P}$ values

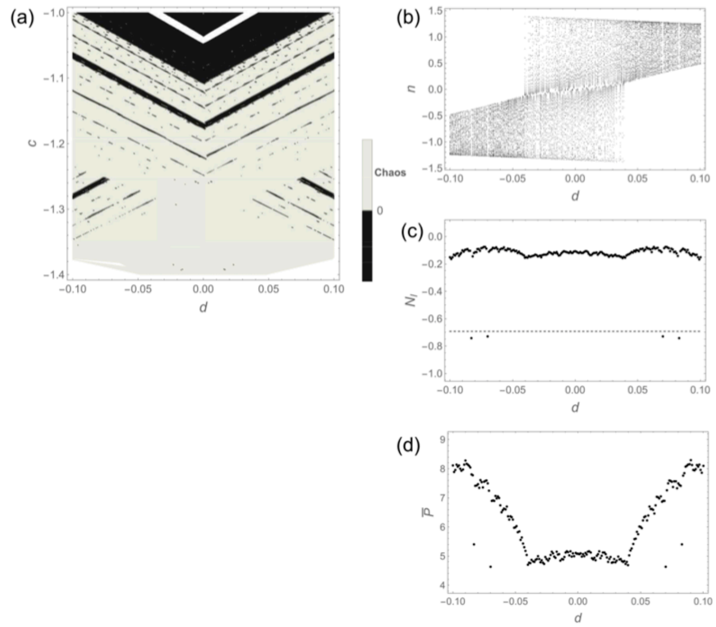

Fig. 12. (a) Contour topography of (N_I+log 2)-values in parameter space of BT ($a = -1, b = 0, n_0 = 0.01$). (b) Corresponding bifurcation diagram ($c = -1.33$). (c) BT's N_I. Gray dotted line is the critical value: $-\ln[2]$. (d) BT's $\overline{P}$.

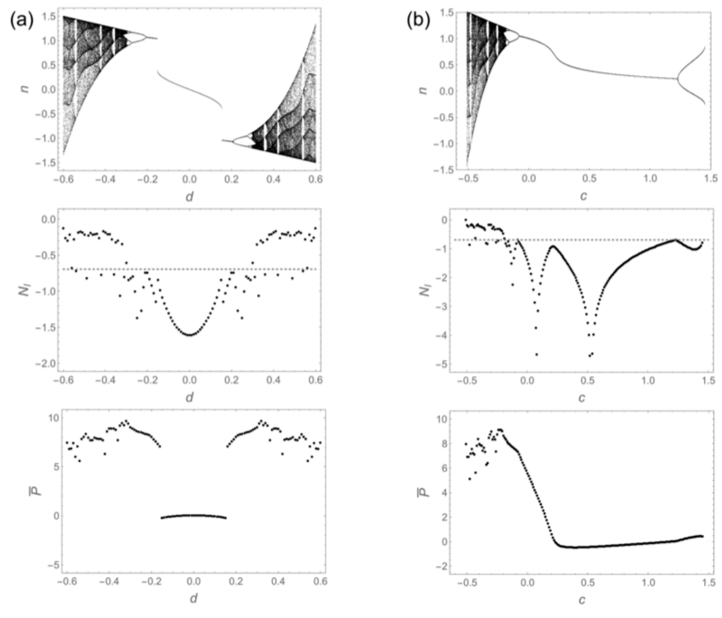

Fig. 13. BT's bifurcation diagram, N_I, and $\overline{P}$. (a) $c = -0.4$. (b) $d = -0.5$. Other conditions are the same as in Fig. 10.

decrease with c. Therefore, the bifurcation diagram shows that the width of the chaotic region increases as c decreases.

Finally, the cusp shown in Fig. 14 warrants consideration. This is an example where the width of chaos does not simply decrease geometrically as $\overline{P}$ increases. To calculate N_I, we use Eqs. (24) and (25); $\overline{P}$ is calculated by substituting Eq. (23) into Eq. (37):

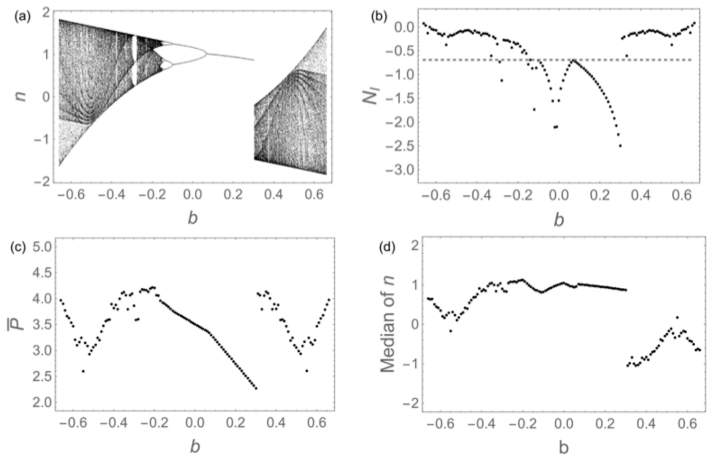

Fig. 14. Cusp's (a) bifurcation diagram, (b) N_I, (c) $\overline{P}$, and (d) median of n. Conditions are the same as in Fig. 3(a).

$$\overline{P} = \frac{1}{T+1}\sum_{t=0}^{T}\left(\frac{1}{4}(-3n_t^4 - 6an_t^2 - 12bn_t + a^2)\right). \tag{39}$$

To calculate n_t, use Eq. (25): $n_{t+1} = -(n_t^3 + an_t + b)$. The calculation conditions remain unchanged from Fig. 3(a). As shown in Fig. 14(a), chaos is present in the area where $b < -0.16$ and $b > 0.31$, and the width of this chaotic region increases toward both ends. Within the region, N_I-values exceed the critical level and little variation is observed; however, around $b \approx \pm 0.5$, they begin to increase (Fig. 14(b)). This contrasts with Figs. 12 and 13, where N_I displays little variation across all chaotic areas. The variation in $\overline{P}$ can be seen in Fig. 14(c). In the chaotic area ($b < -0.16$ and $b > 0.31$), the P-values decrease initially in both directions; however, around $b \approx \pm 0.5$, they begin to increase.

Focusing on the chaotic pattern within the region, $|b| > 0.5$, it is apparent that point density decreases in the lower end of the $b < 0$ region and in the upper end of the $b > 0$ region (Fig. 14(a)). As a result, the effective width of the chaos within the $|b| > 0.5$ region is diminishing. To confirm this, the median value of n_t at each b is plotted in Fig. 14(d). If the density of plot points for each b is constant, the median value will continue to decrease in the $b < 0$ region and increase in the $b > 0$ region. However, the analysis results of Fig. 14(d) show that the median value increases in the $b < 0$ region and decreases in the $b > 0$ region after $b \approx \pm 0.5$. This means that the chaotic region effectively shrinks after $b \approx \pm 0.5$, which corresponds to an increase in N_I (i.e., the chaos trend increases) and $\overline{P}$-values (i.e., becomes localized).

5. Chaos and the non-equilibrium state

Previous research has indicated that the geometric quantities N and P are connected to the non-equilibrium properties of the system [Yamasaki & Yajima, 2016, 2022a]. Accordingly, this section will analyze chaos as a non-equilibrium phenomenon from this standpoint. Swallowtail is taken as an example.

5.1. N_I and $\overline{P}$ in swallowtail

This section considers chaos in swallowtail (hereinafter, SW). In Eq. (3), F is [Thom, 1972; Zeeman, 1977]

$$F_{\mathrm{SW}} = -\partial_n f_{\mathrm{SW}} = -(n^4 + an^2 + bn + c), \tag{40}$$

where a, b, c are constants. Thus, from Eq. (5),

$$g_{\mathrm{SW}} = n^4 + an^2 + bn + c. \tag{41}$$

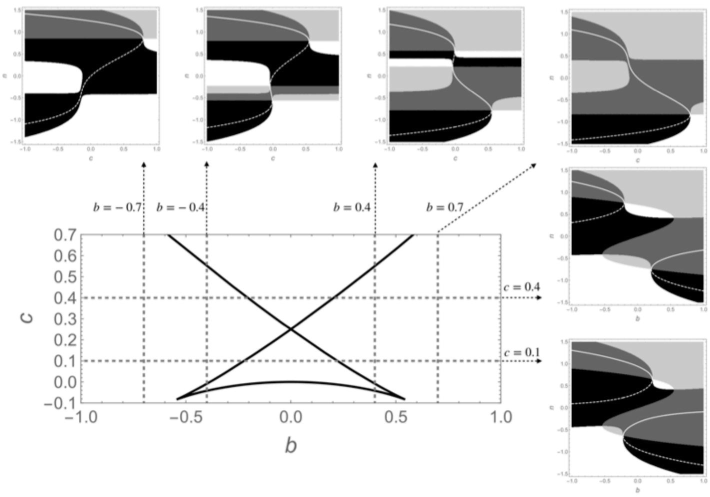

Fig. 15. Swallowtail (SW) singularity ($a = -1$). Equilibrium solution (solid is stable and dotted is unstable) and non-equilibrium stability (gray scale, see main text in Section 3.3) for each parameter are also listed.

We have already shown the following geometric quantities [Yamasaki & Yajima, 2020]:

$$N_{\mathrm{SW}} = 2n^3 + an + \frac{b}{2}, \tag{42}$$

$$P_{\mathrm{SW}} = -2n^6 - 3an^4 - 4bn^3 - 6cn^2 + \frac{1}{4}\left(b^2 - 4ac\right). \tag{43}$$

Conditions where $g_{\mathrm{SW}} = N_{\mathrm{SW}} = 0$ result in a singular pattern of SW in the equilibrium state [Yamasaki & Yajima, 2022b]. From Eqs. (41) and (42), we obtain

$$(b, c) = (-2(an + 2n^3), n^2(a + 3n^2)). \tag{44}$$

A parametric plot for the case $a = -1$ is shown in Fig. 15. For reference, the equilibrium solution for each case and non-equilibrium stability are also shown side by side in Fig. 15.

In SW, the singularity pattern obtained from the equilibrium condition ($g_{SW} = 0$) is axisymmetric (Fig. 15). However, non-equilibrium stability is not necessarily axisymmetric, particularly outside the singularity pattern, unlike cusp and BT [Yamasaki & Yajima, 2020, 2022b]. For example, comparing $b = -0.7$ and $b = 0.7$ in Fig. 15, the stability of the non-equilibrium regions (grayscale) is different.

To confirm this characteristic of SW, the equation corresponding to (44) is given in the cusp and BT. For cusp, from Eqs. (21) and (22), we have

$$(a, b) = (-3n^2, 2n^3). \tag{45}$$

Figure 2(a) shows the corresponding parametric plot. For BT, from Eqs. (31), (32) and $b = 0$, we have

$$(c, d) = (-3an^2 - 5n^4, 2(an^3 + 2n^5)). \tag{46}$$

Figure 9 shows the parametric plot at $a = -1.5$. As shown by even/odd with respect to n in Eqs. (45) and (46), the singularity pattern is symmetrical around the a-axis (($b = 0$)-axis) for cusp (Fig. 2a) and around the c-axis (($d = 0$)-axis) for BT (Fig. 9). This means that in cusp, the singularity pattern gives the same result for $|b|$ in BT as it gives for $|d|$. Because terms b and d are constant parts in the g equation (Eqs. (21) and (31)), they are not in the non-linear connection when g is differentiated by n (Eq. (6)).

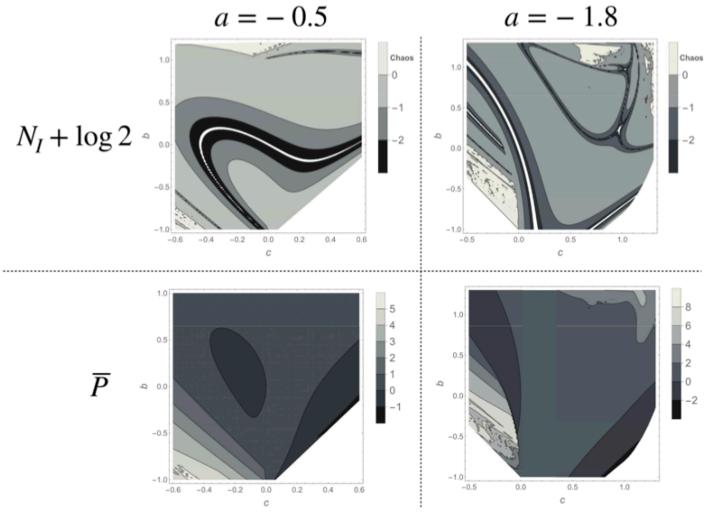

Fig. 16. Contour topography of $(N_I + \log 2)$-values and $\overline{P}$ in parameter space of SW for $a = -0.5$ and $a = -1.8$. $n_0 = 0.01$ in both cases.

When the initial value is small, the distribution of N_I that is related to chaos is symmetrical to the a-axis (($b = 0$)-axis)) for cusp (Fig. 8) and to the c-axis (($d = 0$)-axis)) for BT (Fig. 10).

From Eq. (44), in the case of SW, the even function with respect to n is c, and the odd function is b. Therefore, the singularity pattern is axisymmetric with regard to the c axis, and the singularity pattern (equilibrium pattern) returns the same value for absolute b. However, in contrast to cusp and BT, because b is a non-constant term of g (Eq. (41)), it is explicitly included in the non-linear connection. Thus, both N_I and $\overline{P}$ distributions appear asymmetric (Fig. 16). Naturally, this asymmetry impacts the distribution of chaos occurrence and its development in SW. Here, under the conditions $a = -1$ and $n_0 = 0.01$, Eqs. (12) and (42) are used to calculate N_I, Eqs. (37) and (43) are used to calculate $\overline{P}$, and n_t is calculated using $n_{t+1} = -(n_t^4 + an_t^2 + bn_t + c)$.

In contrast to the singularity pattern obtained under the equilibrium condition, the distribution patterns of N_I and $\overline{P}$ contain significant non-equilibrium information. In other words, the emphasis on non-equilibrium characteristics renders the SW more unique. In the following section, we examine non-equilibrium state asymmetries, with a focus on the growth process of the bifurcation diagrams.

5.2. *Chaos before a dynamic equilibrium state*

During the growth process of the bifurcation diagram, as examined in previous sections, if the initial magnitudes are equal but the signs are opposite, the pattern is reversed (e.g., Figs. 5). The phenomenon of pattern inversion is also a reflection of symmetry. However, in contrast to pattern inversion, reflecting the asymmetry in the non-equilibrium state seen above, SW exhibits a different growth pattern.

For example, in Fig. 17, we present the case of the initial value of $n_0 = \pm 0.5$ under the condition of $a = -1, b = 1.2$. The numbers on the figure describe the t intervals. After a sufficient amount of time elapses ($t = 5001 \sim 5100$), the system achieves a dynamic equilibrium state in which the chaotic patterns formed in the $c > 0$ region converge to approximately the same pattern, regardless of the initial value $n_0 = \pm 0.5$. Meanwhile, during the process of forming these patterns (the non-equilibrium state, $t = 1 \sim 100$), the distinction between the two $n_0 = \pm 0.5$ is prominent. Chaos that exists briefly in non-equilibrium states but disappears in dynamic equilibrium states is also observed. While most research has focused on chaos in dynamical equilibrium systems, the chaos in non-equilibrium systems during the process of reaching dynamical equilibrium is also noteworthy, especially in SW. These instances are significant, as the natural world does not always attain equilibrium (e.g., [Pickett, 1980; Sprugel, 1991; Mori, 2011]).

Furthermore, in the natural world, parameters do not remain constant and multiple parameters are

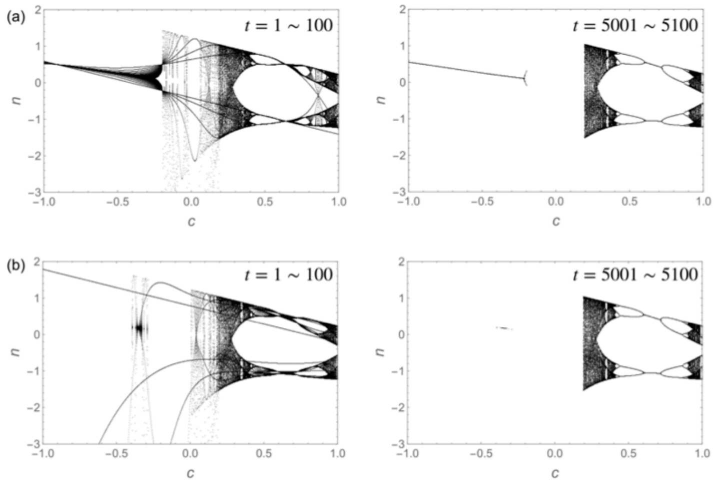

Fig. 17. Bifurcation diagram ($a = -1$, $b = 1.2$) for each t period. (a) $n_0 = 0.5$. (b) $n_0 = -0.5$.

not necessarily independent of one another. In the upcoming section, we will explore the chaotic impact of such discrepancies.

6. Singularity patterns and chaos

6.1. *Bivariate parameters: the simple example*

In contrast to the case of constant parameter variation in the cusp parameter space (see Fig. 2), we consider here the case where the parameters are related to each other. This situation demonstrates diverse patterns (e.g., [Thom, 1972; Golubitsky, & Schaeffer, 1979; Gilmore, 1981]). Our investigation focused on systems where the variables a and b are oscillatory and correlated:

$$a = c_1 \sin[c_2 b] + c_3, \tag{47}$$

where c_1, c_2 and c_3 are parameters. Considering the position of the singularity pattern in relation to the interior and exterior, three typical types, denoted as (a), (b), and (c), can be identified, as shown in Fig. 18. Regarding the catastrophe involved, Figs. 18(b) and (c) are comparable to Fig. 2(b), apart from the observation that the equilibrium solution displays a discrete pattern resembling an egg shape in Fig. 18(b) [Gilmore, 1981].

Figures 18(a),(b), and (c) also depict the outcomes of N_I computations for the three above mentioned patterns from Eqs. (24) and (25). The same calculation method used in Section 3 was employed. In the case of Fig. 18(a), all N_I values fall below the critical value $(-\ln[2])$, thereby indicating the absence of chaos. This means that the information of non-linear connections within the singularity pattern is necessary for chaos to occur under these conditions.

In fact, the internal information in Figs. 18(b) and (c) shows that N_I surpasses the critical value $(-\ln[2])$, resulting in chaos. It is evident that the chaos within the pattern (Fig. 18(c)) is more extensive than that both inside and outside the pattern (Fig. 18(b)). This is caused by low N_I values near the singular point in Fig. 18(b). These findings suggest the frequent occurrence of chaos in bistable states, except near the singular point.

6.2. *Singularity patterns and the chaos-generating region*

The previous section's simple example implies a close relationship between regions of chaos and singularity patterns. To enhance visual clarity, we superimpose the cusp singularity pattern (Eq. (45)) and the distribution of non-linear connections information (Eqs. (24) with (25)) in parameter space (Figs. 19(a)(b)).

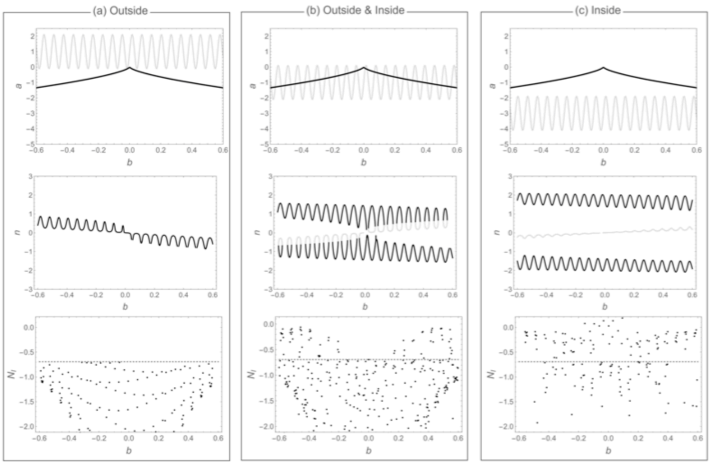

Fig. 18. Cusp's singular pattern, equilibrium solutions (black line is stable solution; gray is unstable solution), and N_I (dotted line represents the critical value) when parameters oscillate ($c_1 = 1, c_2 = 100, n_0 = 0.1$). (a) Outside ($c_3 = 1$). (b) Outside and inside ($c_3 = -1$). (c) Inside ($c_3 = -3$).

Figure 19(a) illustrates that parameters that vary exclusively outside the singular pattern correspond to almost non-chaotic regions. Conversely, parameters that vary both inside and outside the singular pattern can traverse the chaotic region, except in the region close to the singular point. At the singular point, both the equilibrium condition ($g = 0$) and all geometric quantities N, P approach zero [Yamasaki & Yajima, 2022b]. Thus, it is anticipated that the absolute value of the N_I is statistically low around the singularity, and chaos is not expected to occur. Moreover, Fig. 19(b) shows that the cliff (the boundary where the discontinuous transition from chaotic to non-chaotic occurs) and the line of the singularity pattern (the boundary where the discontinuous transition from equilibrium point to equilibrium point occurs) may not coincide.

The same examination was conducted for BT and SW, with the results shown in Figs. 19(c) and (d). A comparison of Fig. 19(c) with Fig. 12(a) highlights that the region where the chaos at both ends merge exists only within the singularity pattern, as described in Section 4. In essence, similar to the cusp, regions where only chaos spreads arise from the utilization of the information of non-linear connections within the singularity. In contrast, the singularity pattern in the case of SW (Fig. 19(d)) appears to have little influence on the generation of chaotic regions, indicating the asymmetry described in Sec. 5. These findings, based on the combination of the distribution of N_I and singular patterns, are summarized in the following.

7. Summary

We examined the correlation between catastrophe and chaos in geometric quantities, using KCC theory in Finsler geometry and numerical analysis in discrete mathematics. The key findings are concisely outlined in the tables presented below.

- Finsler geometric quantities used to analyze catastrophes are applied to chaos analysis, introducing two statistics: non-linear connections information, N_I, and the mean deviation curvature, $\overline{P}$ (Tables 1 and 2). These tables suggest that the geometric statistics of Finsler geometry are also valuable for numerically analyzing discrete chaos systems and can provide a comprehensive description of the relationship between chaos and catastrophe.
- The topographical contours of N_I-values in the parameter space facilitate a clear visualization of the chaotic features in catastrophes, highlighting sudden changes and a dependence on the initial conditions (Table 3). Generally, analyzing systems with multiple parameters, even in one dimension, is more complex. The graphical representation used in this study simplifies the dependence of chaos-generating regions and their pattern changes on the two parameters.

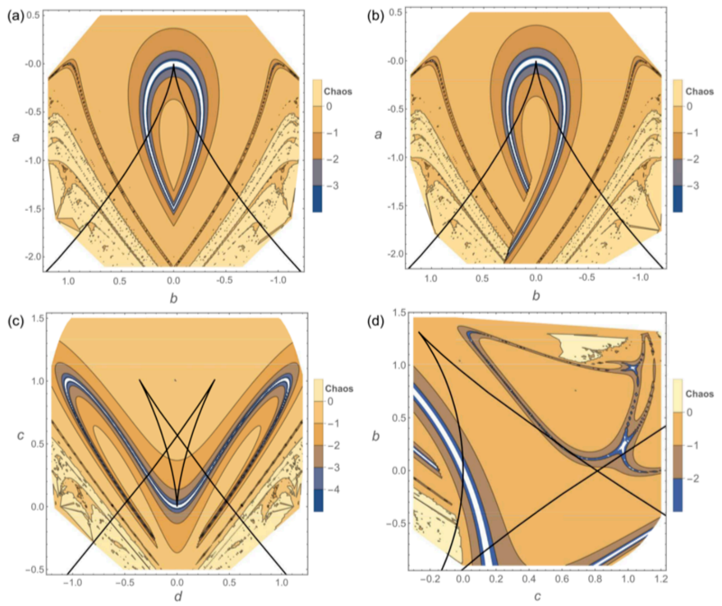

Fig. 19. Superposition of singularity patterns and non-linear connections information. Since (N_I+log 2) values are plotted, the positive regions correspond to chaotic regions. (a) Cusp ($n_0 = 0.01$). (b) Cusp ($n_0 = 0.3$). (c) BT ($a = -1.5, b = 0, n_0 = 0.01$). (d)SW ($a = -1.8, n_0 = 0.01$).

- By superimposing the contour map of N_I-values with the singularity pattern, the pattern of singularities known to constrain the distribution of non-equilibrium stability in catastrophes also constrains the distribution of chaos, typically a non-equilibrium phenomenon (Table 4). This is a geometric summary of the features of systems in which chaos and catastrophe coexist and shows that the two have a complex relationship, constrained by the singularity.
- The asymmetry in SW chaos is less distinguishable in an equilibrated state, but becomes more evident when the system is in a state of non-equilibrium (Figs. 17 and 19(d)). This means that, compared to various other catastrophes, chaos caused by SW can exhibit more complex patterns in the non-equilibrated state.

Table 1: Qualitative characteristics.

	Role in chaos analysis
N_I	Determination based on non-equilibrium stability
$\overline{P}$	Degree of development based on robustness

Table 2: Quantitative characteristics.

	Increase	Decrease	Examples
N_I	$N_I > -\ln[2]$: Chaos	$N_I < -\ln[2]$: Non-chaos	Figs. 1, 3, 6
$\overline{P}$	Relative localization	Relative globalization	Figs. 12∼14

Table 3: Catastrophe properties and contour topography.

	Topographic Features	Examples
Abrupt change	Cliff, Dislocation	Figs. 7, 8, 11
Initial dependence	Reversal of topography	Ibid.

Table 4: Singular(S), topography and chaos.

	Topography	Chaos	Examples
Around S-point	Low elevation	No	Figs. 18, 19
Inside S-pattern	High elevation	Extensive	Figs. 12, 19

References

Ashish, Cao, J., & Chugh, R. [2021] "Discrete chaotification of a modulated logistic system," *Int. J. Bifurcat. Chaos*, **31**, 2150065.

Antonelli, P.L. [1985] *Mathematical essays on growth and the emergence of form*, (University of Alberta Press, Alberta).

Antonelli, P.L., Ingarden, R.S. & Matsumoto, M. [1993] *The theory of sprays and Finsler spaces with applications in physics and biology*, (Kluwer, Dordrecht).

Antonelli,, P.L. & Bucataru, I. [2003] *KCC theory of a system of second order differential equations, in: Handbook of Finsler Geometry*, (Kluwer, Dordrecht).

Antonelli, P.L., Leandro, E.S. & Rutz, S.F. [2014] "Gradient-driven dynamics on Finsler manifolds: the Jacobi action-metric theorem and an application in ecology," *Nonlinear Stud.* **21**, 141–152.

Antonelli, P. L., Rutz, S. F. & Ferreira Jr, G.S. [2019] "Remarks on modelling serial endosymbiosis and evolution of eukaryote tissue formation," *Nonlinear Stud.* **26**, 653–662.

Antonelli, P., Rutz, S., & Strychar, K. B. [2021] "Heat stress on Scleractinian corals: Its symbionts in evolution," *Nonlinear Anal. RWA.* **28**, 189-196.

Bathiany, S., Scheffer, M., Van Nes, E. H., Williamson, M. S., & Lenton, T. M. [2018]. "Abrupt climate change in an oscillating world," *Sci. Rep.* **8**, 5040.

Bröcker, T., & Lander, L. [1975] *Differentiable germs and catastrophes*, (Lect. Note Series, 17, London Math. Soc.).

Boehmer, C.G. & Harko, T. [2010] "Nonlinear stability analysis of the emden-fowler equation," *J. Nonlinera. Math. Phy.* **17**, 503–516.

Brown, C., [1995] *Chaos and catastrophe theories*, (Sage, CA).

Buscarino, A., & Fortuna, L. [2023] "A shifted logistic map. International Journal of Bifurcation and Chaos," *33*, 2330002.

Chen, B., Liu, Y., Wei, Z. & Feng, C. [2020] "New insights into a chaotic system with only a Lyapunov stable equilibrium," *Math. Methods Appl. Sci.* **43**, 9262–9279.

Chen, X., Bao, J., & Yu, H. [2021] "New insights into the extended Malkus-Robbins dynamo," *Chaos Solit. Fractals*, **147**, 110966.

Chen, Y. & Leung, A. Y. T. [2012] *Bifurcation and chaos in engineering*, (Springer, London).

Chen, Y. & Yin, Z. [2019] "The Jacobi stability of a Lorenz-type multistable hyperchaotic system with a curve of equilibria," *Int. J. Bifurcat. Chaos* **29**, 1950062.

Dănilă, B., Harko, T., Mak, M.K., Pantaragphong, P. & Sabău, S.V. [2016] "Jacobi stability analysis of scalar field models with minimal coupling to gravity in a cosmological background," *Adv. High Ene. Phy.* **2016**, p. 26.

Eisenman, I., & Wettlaufer, J. S. [2009] "Nonlinear threshold behavior during the loss of Arctic sea ice," *PNAS*, **106**, 28–32.

Elaydi, S. [2003] "Is the world evolving discretely?," *Adv. Appl. Math*, **31**, 1-9.

Elaydi, S. N. [2007] *Discrete chaos: with applications in science and engineering*, (CRC press, New York).

Gaito, S & G. King, G. [1989] "Chaos on a catastrophe manifold," *Measures of Complexity and Chaos*, eds. N.B. Abraham et al., (Plenum Press, New York), **208**, pp. 235-240.

Geist, K., Parlitz, U., & Lauterborn, W. [1990] "Comparison of different methods for computing Lyapunov exponents," *Prog. Theor. Phys.*, **83**, 875-893.

Ghil, M., & Childress, S. [1987] "Persistent anomalies, blocking and predictability," *Topics in Geophysical Fluid Dynamics: Atmospheric Dynamics, Dynamo Theory, and Climate Dynamics,* (Springer, New York), pp. 125–201.

Gilmore, R. [1981] *Catastrophe theory for scientists and engineers*, (Dover, New York).

Golubitsky, M., & Schaeffer, D. [1979] "Theory for imperfect bifurcation via singularity theory," *Commun. Pure. Appl. Math.* **32**, 21–98.

Gu, J., & Chen, S. [2014] "Nonlinear analysis on traffic flow based on catastrophe and chaos theory," *Discret. Dyn. Nat. Soc.*, **2014**, 1-11.

Gupta, M. K., & Yadav, C. K. [2017] "Jacobi stability analysis of Rössler system," *Int. J. Bifurcat. Chaos*, **27**, 1750056.

Harko, T., Ho, C.Y., Leung, C.S. & Yip, S. [2015] "Jacobi stability analysis of the Lorenz system," *Int. J. Geo. Meth. Mod. Phy.* **12**, 1550081.

Harko, T., Pantaragphong, P. & Sabău, S.V. [2016] "Kosambi-Cartan-Chern (KCC) theory for higher-order dynamical systems," *Int. J. Geo. Meth. Mod. Phy.* **13**, 1650014.

Harko, T. & Sabău, S.V. [2008] "Jacobi stability of the vacuum in the static spherically symmetric brane world models," *Phys. Rev. D.* **77**, 104009.

Hirakui, Y., & Yajima, T. [2021] "Geometrical classification of self-similar motion of two-dimensional three point vortex system by deviation curvature on Jacobi Field," *Adv. Math. Phys.* **2021**, 1–14.

Hirsch, M. W., Smale, S., & Devaney, R. L. [2012] *Differential equations, dynamical systems, and an introduction to chaos.*, (Academic press, London).

Huang, Q., Liu, A. & Liu, Y. [2019] "Jacobi stability analysis of the Chen system," *Int. J. Bifurcat. Chaos* **29**, 1950139.

Jakimowicz, A. [2010] "Catastrophes and chaos in business cycle theory," *Acta Phys. Pol. A*, **117**, 640-646.

Kam, J.K. [1992] "Are chaos and catastrophe theories relevant to environmental sciences?," *J Environ Sci*, **4**, 39-42.

Kumar, M., Mishra, T. N. & Tiwari, B. [2019] "Stability analysis of Navier-Stokes system," *Int. J. Geom. Methods Mod. Phys.*, **16**, 1950157.

Kuznetsov, N., Mokaev, T., Ponomarenko, V., Seleznev, E., Stankevich, N., & Chua, L. [2023] "Hidden attractors in Chua circuit: mathematical theory meets physical experiments," *Nonlinear Dyn.*, **111**, 5859–5887.

Lai, T., Feng, C., Liu, Y., & Liu, A. [2022] "Geometric analysis and onset of chaos for the resonant nonlinear Schrödinger system," *EPJ ST*, **231**, 2133–2142.

Lake, M.J. & Harko, T. [2016] "Dynamical behavior and Jacobi stability analysis of wound strings," *Eur. Phys. J.* **76**, 1–26.

Lenton, T. M., Held, H., Kriegler, E., Hall, J. W., Lucht, W., Rahmstorf, S., & Schellnhuber, H. J., & Lenton, T. M. [2008]. "Tipping elements in the Earth's climate system," *PNAS* **105**, 1786–1793.

Li, J., Zang, H., & Wei, X. [2020] "On the construction of one-dimensional discrete chaos theory based on the improved version of Marotto's theorem," *J. Comput. Appl. Math.*, **380**, 112952.

Liu, A., Chen, B. & Wei, Y. [2020] "Jacobi analysis of a segmented disc dynamo system," *Int. J. Geom. Methods Mod. Phys.* **17**, 2050205.

Liu, Y., Huang, Q. & Wei, Z. [2021a] "Dynamics at infinity and Jacobi stability of trajectories for the Yang-Chen system," *Discrete. Contin. Dyn. Syst. Ser. B* **26**, 3357–3380.

Liu, Y., Li, C., & Liu, A. [2021b] "Analysis of geometric invariants for three types of bifurcations in 2D differential systems," *Int. J. Bifurcat. Chaos*, **31**, 2150105.

Liu, Y., Chen, B., Huang, X., Ye, L., & Wei, Z. [2022a] "Qualitative geometric analysis of traveling wave solutions of the modified equal width Burgers equation," *Math. Models Methods Appl. Sci.*, **45**, 9560–9577.

Liu, Y., Chen, H., Lu, X., Feng, C., & Liu, A. [2022b] "Homoclinic orbits and Jacobi stability on the orbits of Maxwell – Bloch system," *Appl. Anal.* **101**, 4377–4396.

Lynch, S. [2007] *Dynamical systems with applications using Mathematica*, (Birkhäuser, Boston).

May, R. M. [1974] "Biological populations with nonoverlapping generations: stable points, stable cycles, and chaos," *Science* **186**, 645–647.

May, R. M. [1976] "Simple mathematical models with very complicated dynamics," *Nature* **261**, 459–467.

Mori, A. S. [2011] "Ecosystem management based on natural disturbances: hierarchical context and non-equilibrium paradigm," *J. Appl. Ecol.* **48**, 280–292.

Munteanu, F. [2022a] "Analyzing the Jacobi stability of Lü's circuit system," *Symmetry* **14**, 1248.

Munteanu, F. [2022b] "A Study of the Jacobi stability of the Rosenzweig – MacArthur predator – prey system through the KCC geometric Theory," *Symmetry* **14**, 1815.

Munteanu, F., Grin, A., Musafirov, E., Pranevich, A., & Şterbeţi, C. [2023a] "About the Jacobi stability of a generalized Hopf-Langford System through the Kosambi-Cartan-Chern geometric theory," *Symmetry* **15**, 598.

Munteanu, F. [2023b], "On the Jacobi stability of two SIR epidemic patterns with demography," *Symmetry* **15**, 1110.

Nagy, P., & Tasnádi, P. [2013], "Zeeman catastrophe machines as a toolkit for teaching chaos," *Eur. J. Phys.* **35**, 015018.

Oiwa, S. & Yajima, T. [2017] "Jacobi stability analysis and chaotic behavior of nonlinear double pendulum," *Int. J. Geom. Methods Mod. Phys.* **14**, 1750176.

Pickett, S. T. [1980] "Non-equilibrium coexistence of plants," *Bull. Torrey Bot. Club*, **107**, 238–248.

Pisarchik, A. N., & Feudel, U. J. S. [2014] "Control of multistability," *Phys. Rep.*, **540**, 167–218.

Qin, S. Q., Jiao, J. J., & Li, Z. G. [2006] "Nonlinear evolutionary mechanisms of instability of plane-shear slope: catastrophe, bifurcation, chaos and physical prediction," *Rock Mech. Rock Eng.*, **39**, 59-76.

Ramu, S. A., Sankar, T. S., & Ganesan, R. [1994] "Bifurcations, catastrophes and chaos in a pre-buckled beam," *Int. J. Non. Linear Mech.*, **29**, 449–462.

Rinaldi, S., Muratori, S., & Kuznetsov, Y. [1993] "Multiple attractors, catastrophes and chaos in seasonally perturbed predator-prey communities," *Bull. Math. Biol.*, **55**, 15–35.

Sabău, S.V. [2005a] "Some remarks on Jacobi stability," *Nonlinear Anal. TMA.* **63**, e143–e153.

Sabău, S.V. [2005b] "Systems biology and deviation curvature tensor," *Nonlinear Anal. RWA.* **6**, 563–587.

Shukla, J. [1998] "Predictability in the midst of chaos: A scientific basis for climate forecasting," *Science*, **282**, 728-731.

Sprugel, D. G. [1991] "Disturbance, equilibrium, and environmental variability: what is 'natural' vegetation in a changing environment?," *Biol. Conserv.* **58**, 1–18.

Sulimov, V. D., Shkapov, P. M. & Sulimov, A. V. [2018] "Jacobi stability and updating parameters of dynamical systems using hybrid algorithms," *IOP Conf. Ser. Mater. Sci. Eng.* **468**, 012040.

Thom, R. [1972] *Stabilité Structurelle et Morphogénèse*, (Benjamin, New York).

Toth, C. D., O'Rourke, J., & Goodman, J. E. (Eds.). [2017] *Handbook of discrete and computational geometry*, (CRC press, New York).

Wang, F., Liu, T., Kuznetsov, N. V., & Wei, Z. [2021] "Jacobi stability analysis and the onset of chaos in a two-degree-of-freedom mechanical system," *Int. J. Bifurcat. Chaos*, **32**, 2150075.

Wei, Z., Wang, F., Li, H., & Zhang, W. [2022] "Jacobi stability analysis and impulsive control of a 5D self-exciting homopolar disc dynamo," *Discrete. Contin. Dyn. Syst. Ser. B*, **27**, 5029–5045.

Yajima, T., Yamasaki, K., & Nagahama, H. [2018] "Non-holonomic geometric structures of rigid body system in Riemann-Cartan space," *J. Phys. Commun.* **2**, 085008.

Yajima, T., & Nakase, S. [2021] "A geometric interpretation of maximal Lyapunov exponent based on deviation curvature," *Int. J. Geom. Methods Mod. Phys.*, **18**, 2150092.

Yamasaki, K. & Yajima, T. [2013] "Lotka-Volterra system and KCC theory: Differential geometric structure of competitions and predations," *Nonlinear Anal. RWA.* **14**, 1845–1853.

Yamasaki, K. & Yajima, T. [2016] "Differential geometric structure of non-equilibrium dynamics in competition and predation: Finsler geometry and KCC theory," *J. Dynam. Syst. Geomet. Theo.* **14**, 137–153.

Yamasaki, K. & Yajima, T. [2017] "KCC analysis of the normal form of typical bifurcations in one-dimensional dynamical systems: Geometrical invariants of saddle-node, transcritical, and pitchfork bifurcations," *Int. J. Bifurcat. Chaos*, **27**, 1750145.

Yamasaki, K. & Yajima, T. [2020] "KCC analysis of a one-dimensional system during catastrophic shift of the Hill function: Douglas tensor in the nonequilibrium region," *Int. J. Bifurcat. Chaos*, **30**, 2030032.

Yamasaki, K. & Yajima, T. [2022a] "Kosambi – Cartan – Chern stability in the intermediate nonequilibrium region of the Brusselator model," *Int. J. Bifurcat. Chaos*, **32**, 2250016.

Yamasaki, K. & Yajima, T. [2022b] "Kosambi – Cartan – Chern analysis of the nonequilibrium singular point in one-dimensional elementary catastrophe," *Int. J. Bifurcat. Chaos*, **32**, 2250053.

Zeeman, E.C. [1977], *Catastrophe Theory: Selected Papers 1972-1977* (Addison-Wesley, Boston).

Zhang, X. [2023] "When Shimizu-Morioka model meets Jacobi stability analysis: Detecting chaos," *Int. J. Geom. Methods Mod. Phys.*, **20**, 2350033.